molecules

MDPI

Article

Hydrogen Absorption Reactions of Hydrogen Storage Alloy $LaNi_5$ under High Pressure

Toyoto Sato [1,*], Hiroyuki Saitoh [2], Reina Utsumi [2], Junya Ito [1], Yuki Nakahira [2], Kazuki Obana [1], Shigeyuki Takagi [3] and Shin-ichi Orimo [3,4]

[1] Department of Engineering Science and Mechanics, College of Engineering, Shibaura Institute of Technology, Tokyo 135-8548, Japan
[2] Quantum Beam Science Research Directorate, National Institutes for Quantum Science and Technology, Sayo 679-5148, Japan
[3] Institute for Materials Research, Tohoku University, Sendai 980-8577, Japan
[4] Advanced Institute for Materials Research (WPI-AIMR), Tohoku University, Sendai 980-8577, Japan
* Correspondence: toyoto@shibaura-it.ac.jp

Abstract: Hydrogen can be stored in the interstitial sites of the lattices of intermetallic compounds. To date, intermetallic compound $LaNi_5$ or related $LaNi_5$-based alloys are known to be practical hydrogen storage materials owing to their higher volumetric hydrogen densities, making them a compact hydrogen storage method and allowing stable reversible hydrogen absorption and desorption reactions to take place at room temperature below 1.0 MPa. By contrast, gravimetric hydrogen density is required for key improvements (e.g., gravimetric hydrogen density of $LaNi_5$: 1.38 mass%). Although hydrogen storage materials have typically been evaluated for their hydrogen storage properties below 10 MPa, reactions between hydrogen and materials can be facilitated above 1 GPa because the chemical potential of hydrogen dramatically increases at a higher pressure. This indicates that high-pressure experiments above 1 GPa could clarify the latent hydrogen absorption reactions below 10 MPa and potentially explore new hydride phases. In this study, we investigated the hydrogen absorption reaction of $LaNi_5$ above 1 GPa at room temperature to understand their potential hydrogen storage capacities. The high-pressure experiments on $LaNi_5$ with and without an internal hydrogen source (BH_3NH_3) were performed using a multi-anvil-type high-pressure apparatus, and the reactions were observed using in situ synchrotron radiation X-ray diffraction with an energy dispersive method. The results showed that 2.07 mass% hydrogen was absorbed by $LaNi_5$ at 6 GPa. Considering the unit cell volume expansion, the estimated hydrogen storage capacity could be 1.5 times higher than that obtained from hydrogen absorption reaction below 1.0 MPa at 303 K. Thus, 33% of the available interstitial sites in $LaNi_5$ remained unoccupied by hydrogen atoms under conventional conditions. Although the hydrogen-absorbed $LaNi_5H_x$ ($x < 9$) was maintained below 573 K at 10 GPa, $LaNi_5H_x$ began decomposing into NiH, and the formation of a new phase was observed at 873 K and 10 GPa. The new phase was indexed to a hexagonal or trigonal unit cell with $a \approx 4.44$ Å and $c \approx 8.44$ Å. Further, the newly-formed phase was speculated to be a new hydride phase because the Bragg peak positions and unit cell parameters were inconsistent with those reported for the La-Ni intermetallic compounds and La-Ni hydride phases.

Keywords: hydrogen storage material; high-pressure; synchrotron radiation X-ray diffraction

Citation: Sato, T.; Saitoh, H.; Utsumi, R.; Ito, J.; Nakahira, Y.; Obana, K.; Takagi, S.; Orimo, S. Hydrogen Absorption Reactions of Hydrogen Storage Alloy $LaNi_5$ under High Pressure. *Molecules* **2023**, *28*, 1256. https://doi.org/10.3390/molecules28031256

Academic Editor: Maurizio Peruzzini

Received: 19 December 2022
Revised: 25 January 2023
Accepted: 26 January 2023
Published: 27 January 2023

1. Introduction

The utilization of renewable energy is key to reducing the emission of greenhouse gases. Thus, a hydrogen-based society comprising hydrogen production by renewable energy, hydrogen storage, and hydrogen utilization is required for the effective utilization of renewable energy. This indicates that efficient and safe hydrogen storage methods are indispensable in a hydrogen-based society. Pressurized gaseous hydrogen, liquid hydrogen,

and metal hydrides (hydrogen storage materials) are prime candidates for hydrogen storage methods [1–5]. Among them, hydrogen in molecular states (H_2) is stored in the pressurized gaseous and liquid hydrogen, and hydrogen in atomic states (H) is stored in the hydrogen storage materials. Hydrogen storage capacity, an important factor in evaluating hydrogen storage methods, can be defined by its volumetric and gravimetric hydrogen densities. The total amount of hydrogen per volume is referred to as the volumetric hydrogen density, where a larger value indicates a more compact hydrogen storage method. The total amount of hydrogen per mass or weight is referred to as the gravimetric hydrogen density, where a larger value indicates a lighter hydrogen storage method. Notably, the volumetric hydrogen densities of pressurized hydrogen and liquid hydrogen cannot exceed 70 kgH_2/m^3, owing to the repulsion between hydrogen molecules. However, the volumetric hydrogen densities of most hydrogen storage materials can exceed 90 kgH_2/m^3 because hydrogen storage materials are stored hydrogen as atoms, which avoids repulsive interactions between the hydrogen molecules [1,2]. The high volumetric hydrogen densities of hydrogen storage materials are one of the advantages of the three methods. In addition, hydrogen storage materials exhibit reversible hydrogen absorption and desorption reactions under moderate pressure and temperature conditions (e.g., room temperature and below 1 MPa of hydrogen pressure). In the case of pressurized gaseous hydrogen, gaseous hydrogen is compressed under 70 MPa of hydrogen pressure for fuel-cell vehicles. Liquid hydrogen is obtained at 20–30 K. However, practically used hydrogen storage materials, such as $LaNi_5$-based alloys, can undergo hydrogen absorption and desorption reactions at room temperature below 1 MPa of hydrogen pressure. Although hydrogen storage materials have disadvantages, such as low gravimetric hydrogen densities (e.g., gravimetric hydrogen density of $LaNi_5$: 1.38 mass%), they are still considered efficient and safe hydrogen storage methods compared to gaseous or liquid hydrogen storage methods, owing to their high volumetric hydrogen densities and capability to undergo reversible hydrogen absorption and desorption reactions in moderate conditions. Therefore, many hydrogen storage materials have been reported [1–5].

The hydrogen absorption and desorption reactions of hydrogen storage materials involve the reaction of materials under hydrogen gas pressure. Hydrogen absorption reactions correspond to the formation of hydride phases, and hydrogen desorption reactions correspond to the decomposition of the hydride phases [1,2]. In hydrides, hydrogen basically exists in various states, including elemental hydrogen (hydrogen with charge neutral), ionic (protons (H^+) and hydride ions (H^-)), and covalently bonded hydrogen. For this reason, hydrogen storage materials are classified by their respective hydrogen states in their hydrides, of which there are three types: interstitial hydrides with elemental hydrogen; ionic hydrides with hydride ions; and complex hydrides with covalently bonded hydrogen [1–12]. In addition, porous materials adsorb hydrogen on their surfaces as molecular hydrogen (physisorption) [13–15].

Among the hydrides, interstitial hydrides are typical hydrogen storage materials, and some of them (e.g., $LaNi_5$-based alloys) are practically used. The reasons are that ionic hydrides (e.g., MgH_2) and complex hydrides (e.g., $NaAlH_4$) can undergo hydrogen absorption and desorption reactions at relatively higher temperatures (typically several hundred degrees Celsius) and pressures (above several MPa of hydrogen gas pressures) because of thermodynamically stable phases, slow hydrogen absorption, and desorption reaction kinetics although their gravimetric hydrogen densities are higher than interstitial hydrides. Intermetallic compounds are often considered to form interstitial hydrides, which can also undergo stable hydrogen absorption and desorption reactions under moderate conditions, as mentioned above. During the hydrogen absorption reactions of intermetallic compounds, hydrogen atoms are located at the interstitial sites, which are typically octahedral and tetrahedral sites coordinated by six and four metal atoms in their lattices, respectively, while maintaining their atomic metal configurations [1–5]. The absorbed hydrogen atoms in the hydrides are released as hydrogen gas by controlling the pressure and/or temperature of the hydrogen gas.

Among hydrogen storage materials, $LaNi_5$-based alloys of the AB_5 alloy type (A and B are typically lanthanides with high hydrogen affinities and transition metals with low hydrogen affinities, respectively) are well-known as practical hydrogen storage materials because of their ability to undergo reversible hydrogen absorption and desorption reactions at room temperature and below 1 MPa of hydrogen gas pressure. Therefore, many studies have investigated the hydrogen storage properties of $LaNi_5$-based alloys, including the hydrogen absorption and desorption reaction cycles, crystal structures, microstructures, and morphologies [5,16–30]. The crystal structures of $LaNi_5$ before and after hydrogen absorption are shown in Figure 1 [18,21]. $LaNi_5$ has a hexagonal structure with a = 5.013 Å and c = 3.987 Å in the space group *P*6/*mmm* (No. 191) [21]. Although crystal structures for the hydrogen-absorbed phase $LaNi_5H_6$ with different space groups and unit cell parameters have been reported, we refer to a trigonal unit cell with a = 5.410 Å and c = 4.293 Å in the space group *P*31*m* (No. 157) [18] in this paper. In the crystal structure of $LaNi_5H_6$, hydrogen atoms are located at octahedral sites coordinated by two La and four Ni atoms; the tetrahedral sites are coordinated by two La and two Ni atoms. In the octahedral and tetrahedral sites, the site occupancies of the hydrogen atoms are 96% at 3*c* (octahedral sites) and 52% at 6*d* (tetrahedral sites) in the space group *P*31*m* (No. 157), respectively. The gravimetric and volumetric hydrogen densities of $LaNi_5$ are 1.38 mass% and 92 kgH_2/m^3, respectively. Despite the higher volumetric hydrogen density of $LaNi_5$ compared to that of gaseous and liquid hydrogen (less than 70 kgH_2/m^3), it is necessary to improve the low gravimetric hydrogen density.

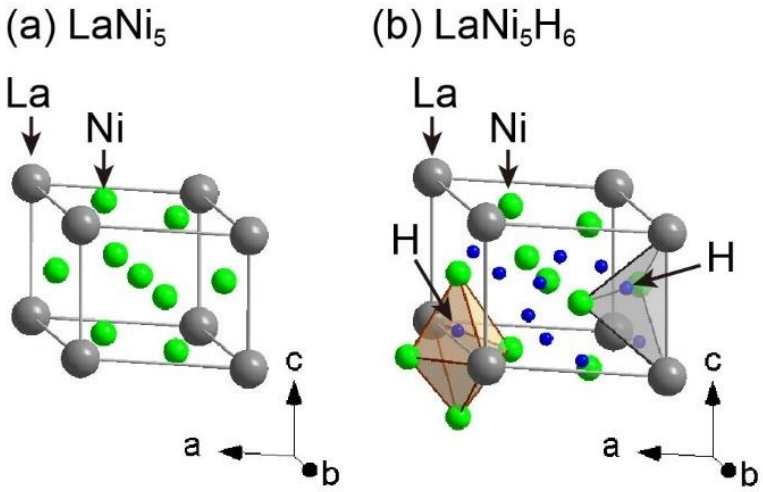

Figure 1. Crystal structures of (**a**) $LaNi_5$ with a = 5.013 Å and c = 3.987 Å in the space group *P*6/*mmm* (No. 191) [21], and (**b**) $LaNi_5H_6$ with a = 5.410 Å and c = 4.293 Å in the space group *P*31*m* (No. 157) [18]. Gray, green, and blue spheres indicate La, Ni, and H atoms, respectively. The brown octahedron and gray tetrahedron denote H atomic sites at 3c and 6d, respectively.

Although studies on hydrogen absorption and desorption reactions in hydrogen storage materials are typically conducted below 10 MPa, hydrogen absorption reactions can be facilitated above 1 GPa because of the drastic increase in the chemical potential of hydrogen [31]. To apply pressures above 1 GPa, multi-anvil-type high-pressure apparatus or diamond anvil cells have often been employed. In the multi-anvil-type high-pressure apparatus experiments, internal hydrogen sources, which supply hydrogen during the high-pressure experiments, are usually enclosed for the hydrogenation reaction (hydrogen absorption) because it is difficult to supply such high pressures using gaseous hydrogen. Hydrogen sources must release hydrogen above 1 GPa at the lowest possible temperature. In addition, the released hydrogen should not be absorbed by the hydrogen sources but by the sample instead. This indicates that the internal hydrogen source did not exhibit a reversible reaction between hydrogen desorption and absorption above 1 GPa. To date, BH_3NH_3 (hydrogen content: 19.6 mass%), a mixture of $NaBH_4$ and $Ca(OH)_2$ (hydrogen

content: 6.3 mass%), AlH_3 (hydrogen content: 10.1 mass%), and $LiAlH_4$ (hydrogen content: 10.6 mass%) have often been used as the internal hydrogen sources. BH_3NH_3 has the highest hydrogen content and releases hydrogen at approximately 373–473 K at ambient pressure, and has the lowest hydrogen release temperature among the candidate internal hydrogen sources. Furthermore, hydrogen sources are generally separated by BN with a hexagonal crystal structure because the released hydrogen from the hydrogen sources can pass through the BN. A high-pressure experiment above 1 GPa enables the synthesis of new hydrides with the potential for hydrogen storage, which is otherwise difficult to synthesize under conventional conditions. Using a multi-anvil-type high-pressure apparatus, in which samples are enclosed with hydrogen sources, novel hydrides such as Mg_7TMH_x (TM: transition metals in groups 4 and 5) and transition metal complex hydrides with alkali or alkaline-earth metals and Al_3FeH_4 have been successfully synthesized [32–39].

Furthermore, synchrotron X-ray and neutron diffraction are important characterization techniques for observing the hydrogen absorption reaction processes and elucidating their mechanisms under high pressure, as reported for hydride formation processes [37–39]. As mentioned above, many intermetallic compounds classified as interstitial hydrides undergo reversible hydrogen absorption and desorption reactions at room temperature and above ambient pressure. This indicates that the hydrogen-absorbed phases (hydride phases) must be observed under hydrogen pressure because the absorbed hydrogen atoms are released from the intermetallic compounds at ambient pressure. To date, many new hydrides with high hydrogen contents have been reported. Most are ionic or complex hydrides, such as hydrogen with intermediate hydrogen states, which can be recovered at ambient pressure because they are thermodynamically stable hydrides. To our knowledge, a typical hydrogen storage material, $LaNi_5$, has not yet been investigated for hydrogen absorption reactions above 1 GPa, although a TiFe with reversible hydrogen absorption and desorption reactions below 10 GPa has been reported [40].

In this study, we conducted hydrogen absorption reactions on $LaNi_5$, a typical hydrogen storage material, above 1 GPa at room temperature, focusing on investigating its potential hydrogen storage capacity.

2. Results and Discussion

2.1. Hydrogen Absorption and Desorption Reactions below 1 MPa

In this study, the hydrogen absorption and desorption of $LaNi_5$ were measured using a Pressure Composition Temperature (PCT) apparatus at 303 K below 1 MPa (Figure 2). The observed hydrogen storage capacity (1.40 mass%) and equilibrium hydrogen absorption and desorption pressures (0.3 and 0.2 MPa, respectively), including hysteresis, which would originate from strain in atomic arrangements, were consistent with those reported by Liang et al. in [24]. Then, the samples were characterized by a conventional X-ray diffraction diffractometer, as shown in Figure 2. Although the preferred orientation (001) at $2\theta \approx 22.2^\circ$, and (002) at $2\theta \approx 45.4^\circ$, and Bragg peak broadening were observed, the Bragg peak positions and unit cell parameters, hexagonal unit cells with a = 5.013(2) Å, and c = 3.988(1) Å obtained by the indexing program TREOR97 [41], were consistent with the simulated X-ray diffraction pattern of $LaNi_5$ with hexagonal unit cells (a = 5.013 Å, and c = 3.987 Å) [21]. This strain was observed by broadening the Bragg peaks in the X-ray diffraction pattern after the hydrogen absorption and desorption reactions, as reported in [22,24,25]. Therefore, this sample was used to observe the hydrogen absorption reactions of $LaNi_5$ at pressures above 1 GPa, which will be discussed in the following section.

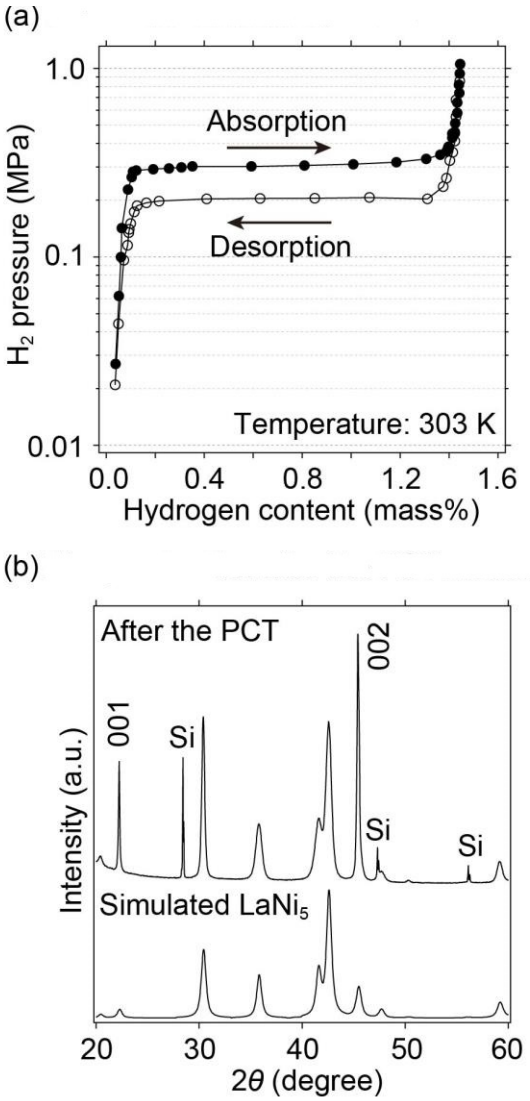

Figure 2. (**a**) PCT curves of $LaNi_5$ measured at 303 K, and (**b**) X-ray diffraction pattern after the PCT measurements with simulated X-ray diffraction pattern of $LaNi_5$. In the X-ray diffraction pattern after the PCT measurement, strong intensities of (001) and (002) reflections originated into a preferred orientation of (00*l*) reflection. Si is added as an internal standard in the X-ray diffraction pattern after the PCT measurement.

2.2. Hydrogen Absorption Reactions at 1.6 GPa and 473 K

$LaNi_5$ with an internal hydrogen source BH_3NH_3 was compressed to 1.6 GPa at room temperature and subsequently heated to 473 K at a heating rate of 100 K/min to release hydrogen. During heating, synchrotron radiation X-ray diffraction patterns were collected every 1 min using the energy-dispersive method, as shown in Figure 3. After 5 min of reaction at 473 K and 1.6 GPa, the Bragg peaks shifted to larger *d*-spacings. This indicates that BH_3NH_3 released hydrogen, which was then absorbed by $LaNi_5$ without yielding byproducts from the reaction between $LaNi_5$ and BN capsules. The amount of absorbed hydrogen is estimated to be approximately 1.70 mass%, corresponding to the formation of $LaNi_5H_{7.3}$, considering the unit cell volume expansion. The details of the hydrogen content considered in this study are discussed later. After the hydrogen absorption reaction was completed, the temperature was lowered to room temperature while maintaining the pressure at 1.6 GPa to observe the hydrogen absorption reaction at room temperature with increasing pressure.

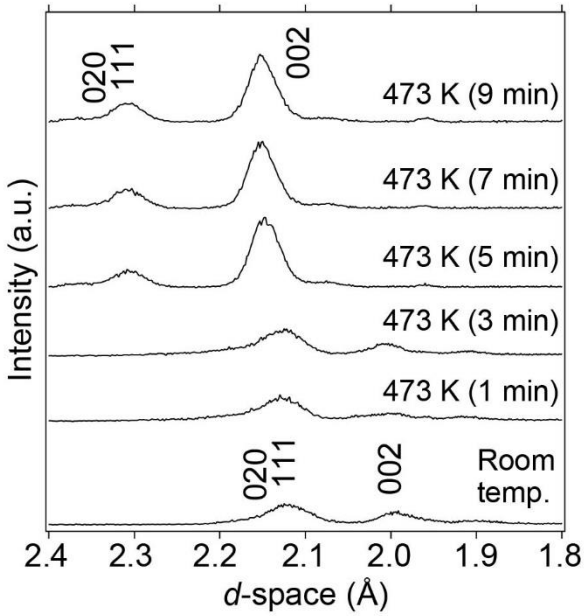

Figure 3. Synchrotron radiation X-ray diffraction patterns of $LaNi_5$ at 473 K and 1.6 GPa focusing on Bragg peaks of the (020), (111), and (002) reflections.

2.3. Hydrogen Absorption Reactions in the Range of 1–10 GPa

Figure 4 shows the synchrotron radiation X-ray diffraction patterns of $LaNi_5$ with and without BH_3NH_3 in the 1.6–10 GPa range at room temperature. High-pressure experiments with and without BH_3NH_3 were performed to observe the hydrogen absorption reaction of $LaNi_5$ and study the unit cell volume expansion of pure $LaNi_5$ with increasing pressure. Although it is difficult to evaluate Bragg peak intensities and widths due to data collection of the X-ray diffraction by the energy-dispersive method and sample positions, the Bragg peak positions of $LaNi_5$ without BH_3NIH_3 shifted to smaller *d*-spacings with increasing pressure, corresponding to the decrease in the unit cell volume as higher pressure was applied. By contrast, the Bragg peak positions of $LaNi_5$ with BH_3NH_3 either remained constant or shifted to larger *d*-spacing despite increasing pressure (1.6 to 6 GPa). This indicated that $LaNi_5$ absorbed hydrogen during compression. Using the X-ray diffraction pattern fitting program, PDindexer [42], the experimentally obtained synchrotron radiation X-ray diffraction patterns were fitted to that of $LaNi_5H_6$ with a hexagonal structure in the space group *P*31*m* (No. 157) [18], and unit cell volumes at each pressure were estimated based on the fitting results. Figure 5 shows the pressure dependence of the unit cell volume. The unit cell volumes of $LaNi_5H_x$ ($LaNi_5$ with BH_3NH_3), predicted $LaNi_5H_6$, and $LaNi_5$ ($LaNi_5$ without BH_3NH_3) were plotted as a function of pressure. The unit cell volume of the predicted $LaNi_5H_6$ was estimated using the unit cell volume of $LaNi_5$ (black data points in Figure 5) and the volume of the hydrogen contribution to $LaNi_5H_6$. The volume of the hydrogen contribution (22.05 $Å^3$/f.u.) was calculated by subtracting the unit cell volume of $LaNi_5$ (87.76 $Å^3$/f.u. [21]) from that of $LaNi_5H_6$ (108.81 $Å^3$/f.u. [18]). As shown in Figure 5, gaps were observed in the unit cell volumes of $LaNi_5H_x$ and the predicted $LaNi_5H_6$. These gaps were proposed to hold extra hydrogen in $LaNi_5H_6$ for the high-pressure experiment. Because the volume of hydrogen contribution was 22.05 $Å^3$/f.u. in $LaNi_5H_6$, each hydrogen atomic contribution was estimated to be 3.68 $Å^3$/f.u. Therefore, the maximum hydrogen storage capacity reaches 2.07 mass% ($LaNi_5H_9$) at 6 GPa. Notably, a similar intermetallic compound, TiFe, with reversible hydrogen absorption and desorption reactions below 10 GPa, also showed the same hydrogen content under normal conditions and higher pressures [40].

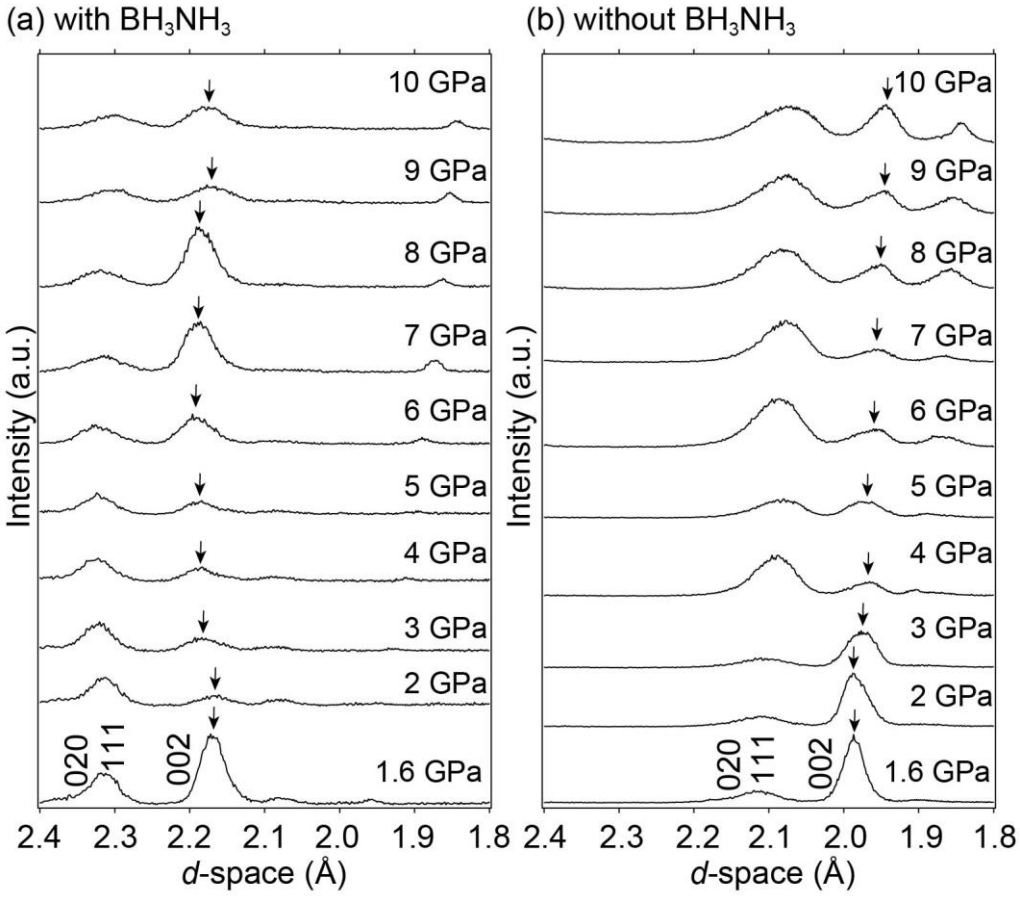

Figure 4. Synchrotron radiation X-ray diffraction patterns of $LaNi_5$ (**a**) with and (**b**) without the internal hydrogen source BH_3NH_3 at room temperature and 1.6–10 GPa focusing on Bragg peaks of the (020), (111), and (002) reflections. Arrows indicate the Bragg peak of (002) at each pressure.

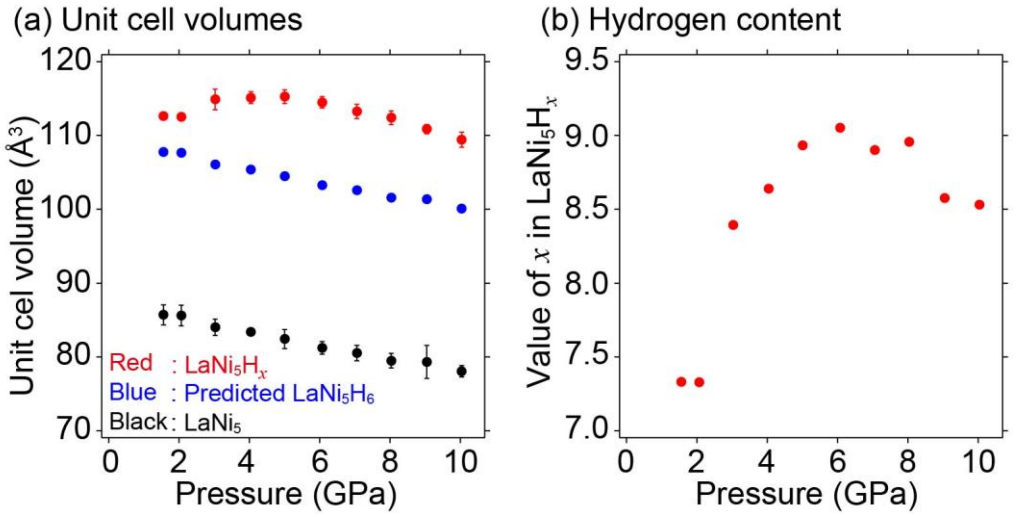

Figure 5. (**a**) Changes in the unit cell volume of $LaNi_5H_x$ ($LaNi_5$ with BH_3NH_3) predicted $LaNi_5H_6$ and $LaNi_5$ without BH_3NH_3, and (**b**) estimated hydrogen content in $LaNi_5H_x$ as a function of pressure.

Subsequently, the sample was heated from room temperature to 873 K at a pressure of 10 GPa to further investigate hydrogen absorption and decomposition (into La hydride (LaH_x) and Ni) reactions at higher temperatures. X-ray diffraction patterns were simultaneously collected during heating. Bragg peaks corresponding to NiH and unknown

Bragg peaks were observed at 873 K and 10 GPa although the hydrogen-absorbed $LaNi_5H_x$ ($x < 9$) was maintained below 573 K at 10 GPa (Figure 6). Using the indexing program TREOR97 [41], the unknown Bragg peaks were indexed to a hexagonal or trigonal unit cell with $a \approx 4.44$ Å and $c \approx 8.44$ Å. The new phase with the hexagonal or trigonal unit cell was speculated to be a new hydride phase because the Bragg peak positions and the phase with the hexagonal or trigonal unit cell did not match those of the La-Ni hydrides and La-Ni intermetallic compounds. Because the new phase could be recovered at an ambient pressure, it might not be classified as an interstitial hydride. The details of the new phase, including its atomic positions and hydrogen content, are currently being investigated.

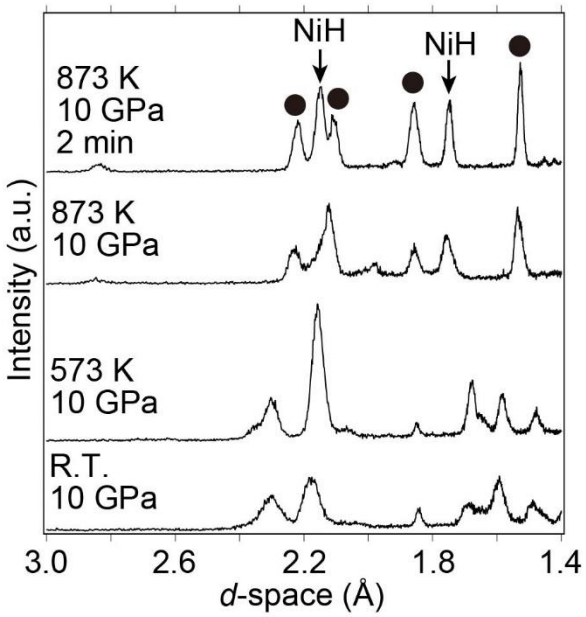

Figure 6. Synchrotron radiation X-ray diffraction patterns from room temperature to 873 K at 10 GPa. The Bragg peaks at 873 K and 10 GPa (2 min) are identified as NiH and a new phase with a hexagonal unit cell (closed circles).

Thus, the high-pressure experiments on $LaNi_5$ suggest that its maximum hydrogen storage capacity of $LaNi_5$ could be 2.07 mass% at 6 GPa, indicating that 33% of the available interstitial sites in $LaNi_5$ remain unoccupied under practical operating conditions. Although hydrogen atoms in $LaNi_5$ occupy octahedral sites coordinated by two La and four Ni atoms and tetrahedral sites coordinated by two La and two Ni atoms (see Figure 1), a small number of hydrogen atoms in $LaNi_5$ with Al ($LaNi_{4.5}Al_{0.5}$) occupied other tetrahedral sites, coordinated by one La and three Ni atoms and by four Ni atoms, as reported by atomic pair distribution function analysis [30]. Therefore, it can be speculated that the hydrogen storage capacities might improve if more hydrogen atoms could occupy the respective tetrahedral sites coordinated by one La, three Ni atoms, and four Ni atoms. To increase the hydrogen atomic occupancies at the tetrahedral sites, replacing multiple metal atoms, which have a larger radius and higher affinity for hydrogen than Ni atoms, with Ni atomic sites might lead to increased amounts of hydrogen atoms in such tetrahedral sites.

3. Materials and Methods

Pieces of $LaNi_5$ (Japan Metals & Chemicals Co., Ltd., Tokyo, Japan) were used in this study. The hydrogen storage properties of $LaNi_5$ at 303 K and below 1 MPa of hydrogen gas pressure were confirmed by PCT measurements (Japan Metals & Chemicals Co., Ltd.). Before the PCT measurement, five cycles of hydrogen absorption and desorption reactions on $LaNi_5$ were performed at room temperature under 1 MPa of hydrogen gas pressure and subsequently under vacuum for activation after heat treatment at 623 K for 3 h. After the PCT measurements, the samples were characterized by powder X-ray diffraction, which

was conducted on a Rigaku SmartLab X-ray diffractometer (Tokyo, Japan) using Cu Kα radiation (λ = 1.540593 Å for $K\alpha_1$ and λ = 1.544414 Å for $K\alpha_2$). The samples were handled in an Ar-gas-filled glovebox with an O_2 content < 1 ppm to prevent (hydro)oxidation.

The hydrogen absorption reactions of $LaNi_5$ at room temperature and above 1 GPa were observed using a multi-anvil-type high-pressure apparatus combined with synchrotron radiation X-ray diffraction at the BL14B1 beamline of SPring-8 in Japan. Before the high-pressure experiment, $LaNi_5$ was activated by heat treatment at 623 K for 3 h, and hydrogen absorption and desorption reactions as the same processes with the PCT measurement at 303 K, as mentioned above. Activated $LaNi_5$ was placed in a BN capsule enclosed by an internal hydrogen source, BH_3NH_3 (Sigma-Aldrich, 97%, St. Louis, MO, USA). The weight ratio of $LaNi_5$ to BH_3NH_3 was approximately 3:2. The sample and the internal hydrogen source were enclosed in a NaCl hydrogen-sealing capsule. The sample cell used in this study was based on that used by Saitoh et al. [38]. The hydrogen release reactions of BH_3NH_3 above 1 GPa have been described in [43,44]. Synchrotron radiation X-ray diffraction patterns were collected during high-pressure experiments using energy-dispersive X-ray diffraction. In high-pressure experiments, diffracted X-rays were obtained using a Ge solid-state detector mounted on a goniometer. The *d*-space of the lattice was obtained using Bragg's law:

$$d = \frac{hc}{2E \sin\theta} \quad (1)$$

where:

h: Planck constant;

c: Speed of light;

E: Energies of the diffracted X-ray;

θ: 3° (diffraction angle 2θ was fixed at 6° in this experiment).

High-pressure experiments on $LaNi_5$ without an internal hydrogen source were also performed using the same procedure to compare the hydrogen absorption reactions. For these cases, BN was used instead of the internal hydrogen source.

In addition, the Bragg peaks in the experimentally obtained synchrotron radiation X-ray diffraction patterns were indexed using TREOR97 [41] and identified using PDindexer [42].

4. Conclusions

In this study, we investigated the hydrogen absorption and desorption reactions of $LaNi_5$ below 1 MP at 303 K and above 1 GPa at room temperature to determine its potential hydrogen storage capacities. High pressures above 1 GPa were induced using a multi-anvil-type high-pressure apparatus, and the hydrogen absorption reactions of $LaNi_5$ above 1 GPa were observed using in situ synchrotron radiation X-ray diffraction with an energy dispersive method at the BL14B1 beamline of SPring-8 in Japan. Although $LaNi_5$ absorbed up to 1.40 mass% hydrogen, of which $LaNi_5H_6$ was formed below 1 MPa at 303 K, the results suggested that the hydrogen storage capacity increased with increasing pressure up to 6 GPa. Considering the unit cell volumes of hydrogen-absorbed $LaNi_5$ phase $LaNi_5H_x$ ($LaNi_5$ with an internal hydrogen source), predicted $LaNi_5H_6$ and $LaNi_5$ (without an internal hydrogen source). The final amount of $LaNi_5$ reached 2.07 mass%, corresponding to the formation of $LaNi_5H_9$ at 6 GPa and room temperature. This indicated that approximately 33% of the available interstitial sites in $LaNi_5$ remained unoccupied by hydrogen atoms under practical operating conditions. The locations of the unoccupied hydrogen atomic sites were speculated to be in tetrahedral sites coordinated by one La, three Ni atoms, and four Ni atoms because small amounts of hydrogen could be located at the tetrahedral sites when a part of Ni was replaced with Al. To increase the hydrogen atomic occupancies at the tetrahedral sites, replacing multiple metal atoms, which have a larger radius and higher affinity for hydrogen than Ni atoms, with Ni atomic sites might

lead to increased amounts of hydrogen atoms in unoccupied hydrogen atomic sites under normal conditions.

While increasing the temperature from room temperature to 873 K at 10 GPa, the hydrogen-absorbed phase $LaNi_5H_x$ ($x < 9$) decomposed to form NiH and a new phase at 873 K. The new phase was indexed to a hexagonal or trigonal unit cell with $a \approx 4.44$ Å and $c \approx 8.44$ Å. It was speculated to be a new hydride phase because its Bragg peak positions were inconsistent with La-Ni Intermetallic compounds and La-Ni hydrides.

Author Contributions: Conceptualization, T.S., H.S., S.T. and S.O.; methodology, T.S. and H.S.; formal analysis, T.S., H.S. and J.I.; investigation, T.S., H.S., R.U., J.I., K.O. and Y.N.; data curation, T.S., H.S., R.U. and J.I.; writing—original draft preparation, T.S.; writing—review and editing, T.S., H.S., R.U., J.I., K.O., Y.N., S.T. and S.O.; visualization, T.S.; supervision, T.S.; project administration, T.S.; funding acquisition, T.S., H.S. and S.O. All authors have read and agreed to the published version of the manuscript.

Funding: This research was funded by MEXT/JSPS KAKENHI (22H01817, JP18H05513 ("Hydrogenomics")), GIMRT Program of the Institute for Materials Research, Tohoku University (Proposal No. 202112-RDKGE-0012), and JST SICORP (JPMJSC 1802).

Institutional Review Board Statement: Not applicable.

Informed Consent Statement: Not applicable.

Data Availability Statement: Not applicable.

Acknowledgments: This research was supported by MEXT/JSPS KAKENHI (22H01817, JP18H05513 ("Hydrogenomics")) and the GIMRT Program of the Institute for Materials Research, Tohoku University (Proposal No. No. 202112-RDKGE-0012) and JST SICORP (JPMJSC 1802). Synchrotron X-ray radiation experiments at SPring-8 were supported by the QST Advanced Characterization Nanotechnology Platform under the remit of the Nanotechnology Platform of the Ministry of Education, Culture, Sports, Science, and Technology MEXT, Japan (Proposal No. JPMXP09A21QS0031, No. JPMXP1222QS0007, and no. JPMXP1222QS0117). The synchrotron radiation X-ray diffraction experiments were performed using a QST experimental station at the QST beamline BL14B1 and SPring-8, with the approval of the Japan Synchrotron Radiation Research Institute JASRI (Proposal No. 2021B3694, No. 2022A3694, and No. 2022B3694).

Conflicts of Interest: The authors declare no conflict of interest.

Sample Availability: Samples of the compounds are available from the authors.

References

1. Schlapbach, L.; Züttel, A. Hydrogen-Storage Materials for Mobile Applications. *Nature* **2001**, *414*, 353–358. [CrossRef] [PubMed]
2. Züttel, A. Materials for Hydrogen Storage. *Mater. Today* **2003**, *6*, 24–33. [CrossRef]
3. Crivello, J.-C.; Dam, B.; Denys, R.V.; Dornheim, M.; Grant, D.M.; Huot, J.; Jensen, T.R.; de Jongh, P.; Latroche, M.; Milanese, C.; et al. Review of Magnesium Hydride–Based Materials: Development and Optimisation. *Appl. Phys. A* **2016**, *122*, 97. [CrossRef]
4. Hirscher, M.; Yartys, V.A.; Baricco, M.; Bellosta von Colbe, J.; Blanchard, D.; Bowman, R.C.; Broom, D.P.; Buckley, C.E.; Chang, F.; Chen, P.; et al. Materials for Hydrogen-Based Energy Storage Past, Recent Progress and Future Outlook. *J. Alloys Compd.* **2020**, *827*, 153548. [CrossRef]
5. Pasquini, L.; Sakaki, S.; Akiba, E.; Allendorf, M.D.; Cho, Y.W.; Alvares, E.; Ares, J.D.; Badai, D.; Bricco, M.; von Colbe, J.B.; et al. Magnesium- and Intermetallic Alloys-Based Hydrides for Energy Storage: Modelling, Synthesis and Properties. *Prog. Energy* **2022**, *4*, 032007. [CrossRef]
6. Orimo, S.; Nakamori, Y.; Eliseo, J.R.; Züttel, A.; Jensen, C.M. Complex Hydrides for Hydrogen Storage. *Chem. Rev.* **2007**, *107*, 4111–4132. [CrossRef] [PubMed]
7. Eberle, U.; Felderhoff, M.; Schüth, F. Chemical and Physical Solutions for Hydrogen Storage. *Angew. Chem. Int. Ed.* **2009**, *48*, 6608–6630. [CrossRef]
8. Takagi, S.; Orimo, S. Recent Progress in Hydrogen-Rich Materials from the Perspective of Bonding Flexibility of Hydrogen. *Scr. Mater.* **2015**, *109*, 1–5. [CrossRef]
9. Sato, T.; Takagi, S.; Deledda, S.; Hauback, B.C.; Orimo, S. Extending the Applicability of the Goldschmidt Tolerance Factor to Arbitrary Ionic Compounds. *Sci. Rep.* **2016**, *6*, 23592. [CrossRef] [PubMed]

10. Sato, T.; Mochizuki, T.; Ikeda, K.; Honda, T.; Otomo, T.; Sagayama, H.; Yang, H.; Luo, W.; Lombardo, L.; Züttel, A.; et al. Crystal Structural Investigations for Understanding the Hydrogen Storage Properties of $YMgNi_4$–Based Alloys. *ASC Omega* **2020**, *5*, 31192–31198. [CrossRef]
11. Sato, T.; Orimo, S. The Crystal Structures in Hydrogen Absorption Reactions of $REMgNi_4$-Based Alloys (RE: Rare-earth metals). *Energies* **2021**, *14*, 8163. [CrossRef]
12. Sato, T.; Ikeda, K.; Honda, T.; Daemen, L.L.; Cheng, Y.; Otomo, T.; Sagayama, H.; Ramirez–Cuesta, A.J.; Takagi, S.; Kono, T.; et al. Effect of Co Substitution on Hydrogen Absorption and Desorption Reactions of $YMgNi_4$-based Alloys. *J. Phys. Chem. C* **2022**, *126*, 16943–16951. [CrossRef]
13. Zhang, L.; Allendorf, M.D.; Balderas–Xicohténcatl, R.; Broom, D.P.; Fanourgakis, G.S.; Froudakis, G.E.; Gennett, T.; Hurst, K.E.; Ling, S.; Milanese, C.; et al. Fundamentals of Hydrogen Storage in Nanoporous Materials. *Prog. Energy* **2022**, *4*, 042013. [CrossRef]
14. Mehrabi, M.; Parvin, P.; Reyhani, A.; Mortazavi, S.Z. Hydrogen Storage in Multi-Walled Carbon Nanotubes Decorated with Palladium Nanoparticles using Laser Ablation/Chemical Reduction Methods. *Mater. Res. Express* **2017**, *4*, 095030. [CrossRef]
15. Mortazavi, S.Z.; Reyhani, A.; Mirershadi, S. Hydrogen Storage Properties of Multi-Walled Carbon Nanotubes and Carbon Nano-Onions Grown on Single and Bi–Catalysts including Fe, Mo, Co and Ni Supported by MgO. *Int. J. Hydrogen Energy* **2017**, *41*, 24885–24896. [CrossRef]
16. Van Mal, H.H.; Buschow, K.H.J.; Miedema, A.R. Hydrogen Absorption in $LaNi_5$ and Related Compounds: Experimental Observations and Their Explanation. *J. Less-Common Met.* **1974**, *35*, 65–76. [CrossRef]
17. Boser, O. Hydrogen Sorption in $LaNi_5$. *J. Less-Common Met.* **1976**, *46*, 91–99. [CrossRef]
18. Fischer, P.; Furrer, A.; Busch, G.; Schlapbach, L. Neutron Scattering Investigations of the LaNi5 Hydrogen Storage System. *Halv. Phys. Acta* **1977**, *50*, 421–430.
19. Percheron-Guégan, A.; Lartigue, C.; Achard, J.C. Correlations Between the Structural Properties, the Stability and the Hydrogen Content of Substituted $LaNi_5$ Compounds. *J. Less-Common Met.* **1985**, *109*, 287–309. [CrossRef]
20. Sakai, T.; Oguro, K.; Miyamura, H.; Kuriyama, N.; Kato, A.; Ishikawa, H.; Iwakura, C. Some Factors Affecting the Cycling Lives of $LaNi_5$-based Alloy Electrodes of Hydrogen Batteries. *J. Less-Common Met.* **1990**, *161*, 193–202. [CrossRef]
21. Kisi, E.H.; Buckley, C.E.; Gray, E.M.A. The Hydrogen Activation of $LaNi_5$. *J. Alloys Compd.* **1992**, *185*, 369–384. [CrossRef]
22. Nakamura, Y.; Oguro, K.; Uehara, I.; Akiba, E. X-ray Diffraction Peak Broadening and Degradation in $LaNi_5$-Based Alloys. *Int. J. Hydrog. Energy* **2000**, *25*, 531–537. [CrossRef]
23. Černý, R.; Joubert, J.-M.; Latroche, M.; Percheron-Guégan, A.; Yvon, K. Anisotropic Diffraction Peak Broadening and Dislocation Substructure in Hydrogen-Cycled $LaNi_5$ and Substitutional Derivatives. *J. Appl. Cryst.* **2000**, *33*, 999–1005. [CrossRef]
24. Liang, G.; Huot, J.; Scchulz, R. Hydrogen Storage Properties of the Mechanically Alloyed $LaNi_5$-based Materials. *J. Alloys Compd.* **2001**, *320*, 133–139. [CrossRef]
25. Joubert, J.-M.; Latroche, M.; Černý, R.; Percheron-Guégan, A.; Yvon, K. Hydrogen Cycling Induced Degradation in $LaNi_5$–type Materials. *J. Alloys Compd.* **2002**, *330–332*, 208–214. [CrossRef]
26. Décampsa, B.; Joubert, J.-M.; Céry, R.; Percheron–Guégan, A. TEM Study of the Dislocations Generated by Hydrogen Absorption/Desorption in $LaNi_5$ and Derivatives. *J. Alloys Compd.* **2005**, *404–406*, 570–575. [CrossRef]
27. Liu, W.; Aguey-Zinsou, K.-F. Low Temperature Synthesis of $LaNi_5$ Nanoparticles for Hydrogen Storage. *Int. J. Hydrogen Energy* **2015**, *41*, 1679–1687. [CrossRef]
28. Faisal, M.; Balani, K.; Subramaniam, A. Cross–Sectional TEM Investigation of Mg–$LaNi_5$–Soot Hybrids for Hydrogen Storage. *Int. J. Hydrogen Energy* **2021**, *46*, 5507–5519. [CrossRef]
29. Joubert, J.-M.; Paul-Boncour, V.; Cuevas, F.; Zhang, J.; Latroche, M. $LaNi_5$ Related AB_5 Compounds: Structure, Properties and Applications. *J. Alloys Compd.* **2021**, *862*, 158163. [CrossRef]
30. Ikeda, K.; Ohshita, H.; Otomo, T.; Sakaki, K.; Kim, H.; Nakamura, Y.; Machida, A.; Von Dreele, R.B. Pressure Cells for in situ Neutron Total Scattering: Time and Real–Space Resolution during Deuterium Absorption. *J. Appl. Cryst.* **2022**, *55*, 1631–1639. [CrossRef]
31. Sugimoto, H.; Fukai, Y. Solubility of Hydrogen in Metals under High Hydrogen Pressures: Thermodynamical Calculations. *Acta Metall. Mater.* **1992**, *40*, 2327–2336. [CrossRef]
32. Moser, D.; Bull, D.J.; Sato, T.; Noréus, D.; Kyoi, D.; Sakai, T.; Kitamura, N.; Yusa, H.; Taniguchi, T.; Kalisvaart, W.P.; et al. Structure and Stability of High Pressure Synthesized Mg–TM Hydrides (TM = Ti, Zr, Hf, V, Nb and Ta) as Possible New Hydrogen Rich Hydrides for Hydrogen Storage. *J. Mater. Chem.* **2009**, *19*, 8150–8161. [CrossRef]
33. Saitoh, H.; Takagi, S.; Matsuo, M.; Iijima, Y.; Endo, N.; Aoki, K.; Orimo, S. Li_4FeH_6: Iron-Containing Complex Hydride with High Gravimetric Hydrogen Density. *APL Mater.* **2014**, *2*, 076103. [CrossRef]
34. Takagi, S.; Iijima, Y.; Sato, T.; Saitoh, H.; Ikeda, K.; Otomo, T.; Miwa, K.; Ikeshoji, T.; Aoki, K.; Orimo, S. True Boundary for the Formation of Homoleptic Transition-Metal Hydride Complexes. *Angew. Chem. Int. Ed.* **2015**, *54*, 5650–5653. [CrossRef]
35. Takagi, S.; Iijima, Y.; Sato, T.; Saitoh, H.; Ikeda, K.; Otomo, T.; Miwa, K.; Ikeshoji, T.; Orimo, S. Formation of Novel Transition Metal Hydride Complexes with Ninefold Hydrogen Coordination. *Sci. Rep.* **2017**, *7*, 44253. [CrossRef]
36. Spektor, K.; Crichton, W.A.; Filippov, S.; Klarbring, J.; Simak, S.I.; Häussermann, U. Na-Ni-H Phase Formation at High Pressures and High Temperatures: Hydrido complexes $[NiH_5]^{3-}$ Versus the perovskite $NaNiH_3$. *ACS Omega* **2020**, *5*, 8730–8743. [CrossRef] [PubMed]

37. Spektor, K.; Crichton, W.A.; Filippov, S.; Simak, S.I.; Häussermann, U. Na_3FeH_7 and Na_3CoH_6: Hydrogen-Rich Complex Transition Metal Hydrides from High Pressure Synthesis. *Inorg. Chem.* **2020**, *59*, 16467–16473. [CrossRef]
38. Saitoh, H.; Sato, T.; Tanikami, M.; Ikeda, K.; Machida, A.; Watanuki, T.; Taguchi, T.; Yamamoto, S.; Yamaki, T.; Takagi, S.; et al. Hydrogen Storage by Earth-Abundant Metals, Synthesis and Characterization of $Al_3FeH_{3.9}$. *Mater. Des.* **2021**, *208*, 109953. [CrossRef]
39. Utsumi, R.; Morimoto, M.; Saitoh, H.; Watanuki, T.; Sato, T.; Takagi, S.; Orimo, S. In situ Synchrotron Radiation X-ray Diffraction Measurements of Fe–Mo Alloy Hydrides Formed under High Pressure and High Temperature. *J. Alloys Compd.* **2022**, *893*, 162300. [CrossRef]
40. Endo, N.; Saita, I.; Nakamura, Y.; Saitoh, H.; Machida, A. Hydrogenation of a TiFe-based alloy at High Pressure and Temperature. *Int. J. Hydrogen Energy* **2015**, *40*, 3283–3287. [CrossRef]
41. Werner, P.-E.; Eriksson, L.; Westdahl, M. TREOR, A Semi–Exhaustive Trial–and–Error Powder Indexing Program for All Symmetries. *J. Appl. Crystallogr.* **1985**, *18*, 367–370. [CrossRef]
42. Seto, Y.; Haname, D.; Nagai, T.; Sata, N. Development of a Software Suite on X-ray Diffraction Experiments. *Rev. High Pressure Sci. Technol.* **2010**, *20*, 269–276. [CrossRef]
43. Nylén, J.; Sato, T.; Soignard, E.; Yarger, J.L.; Stoyanov, E.; Häussermann, U. Thermal Decomposition of Ammonia Borane at High Pressures. *J. Chem. Phys.* **2009**, *131*, 104506. [CrossRef]
44. Nylén, J.; Eriksson, L.; Benson, D.; Häussermann, U. Characterization of a High pressure, High Temperature Modification of Ammonia Borane (BH_3NH_3). *J. Chem. Phys.* **2013**, *139*, 054507. [CrossRef] [PubMed]